

Importance of packing in spiral defect chaos

KAPILANJAN KRISHAN

Department of Physics and Astronomy, University of California-Irvine, Irvine,
California 92697-4575, USA
E-mail: kkrishan@uci.edu

MS received 18 August 2007; revised 30 October 2007; accepted 16 November 2007

Abstract. We develop two measures to characterize the geometry of patterns exhibited by the state of spiral defect chaos, a weakly turbulent regime of Rayleigh–Bénard convection. These describe the packing of contiguous stripes within the pattern by quantifying their length and nearest-neighbor distributions. The distributions evolve towards a unique distribution with increasing Rayleigh number that suggests power-law scaling for the dynamics in the limit of infinite system size. The techniques are generally applicable to patterns that are reducible to a binary representation.

Keywords. Spiral defect chaos; scaling

PACS Nos 47.52.+j; 05.45.-a

1. Introduction

Characterizing the geometry exhibited by a system plays a fundamental role in physics. For example, crystal structures are associated with underlying symmetries that determine many material properties. Often, it is not easy to obtain parameters such as lattice constants, number of nearest-neighbors, etc. in the absence of underlying symmetries. This is particularly true for spatially extended chaotic systems displaying patterns comprising of many length and time scales. Developing measures that can quantify structural properties spanning multiple scales in a robust and consistent way is expected to provide key insights into the dynamics of these systems.

Fluid flows exhibit patterns with rich dynamical behavior in response to external driving. In the classical example of Rayleigh–Bénard convection, a fluid layer held in a vertical temperature gradient undergoes a transition from conductive heat transfer to convective flow. The convection pattern occurring across the fluid layer was described as the linear instability of the conducting state by Rayleigh [1] and parametrized by a dimensionless number known as the Rayleigh number, $R = g\alpha d^3 \Delta T / (\nu\kappa)$. Here g is the acceleration due to gravity, α is the thermal expansion coefficient, d is the thickness of the fluid layer, ΔT is the vertical

temperature difference across the fluid, ν is the kinematic viscosity and κ is the thermal diffusivity of the fluid.

Just above a critical temperature difference, ΔT_c , convective rolls result in a stable, stationary striped pattern. This critical temperature difference corresponds to a critical Rayleigh number, R_c , and the pattern has a critical onset wavelength. The critical Rayleigh number and critical wavelength of the pattern were shown to be universal constants at the onset of the convective instability. Often, a reduced control parameter, $\epsilon = (\Delta T - \Delta T_c)/\Delta T_c$ is used to parametrize the temperature difference, with convection occurring when $\epsilon > 0$. Increasing the Rayleigh number beyond R_c results in time-dependent and turbulent patterns through secondary instabilities of the convective rolls. The stable band of stable and stationary wave vectors between the primary convective instability and secondary instabilities has been predicted by Busse [2].

In Rayleigh–Bénard convection, the externally imposed temperature gradient provides a constant flux of energy through the system and is dissipated within the fluid primarily by thermal conduction and viscous dissipation. The relative strengths of the two dissipation mechanisms is parametrized by the Prandtl number ($\text{Pr} = \nu/\kappa$) and is of order unity for gases, making the patterns they exhibit of interest. In particular, at low Prandtl numbers, roll curvature in the horizontal plane can result in long-range pressure gradients that result in mean flows within the system. These systems therefore show significantly different patterns from fluids with high Prandtl numbers. A review of recent advances in Rayleigh–Bénard convection is found in [3] and references therein.

We characterize patterns obtained from experiments on Rayleigh–Bénard convection [4] in the state of spiral defect chaos, a classical example of spatio-temporal chaos [5–8]. The striped patterns exhibited during spiral defect chaos (see figure 1) are time-dependent with widespread defect formation resulting in the pinch-off and merger of the stripes [9,10]. It was shown that the chaos in the pattern is centered about defect nucleations [11], underlining the importance of local properties [12]. A pivotal study using numerical simulations determined that spiral defect chaos is extensively chaotic, in that the fractal dimension is proportional to the system size [11]. However, there are few quantitative measures of the impact of local instabilities and defects on the large scale geometry of the pattern. The characterizations developed in this paper obtain distributions for the length scales of stripes as well as nearest-neighbor distributions that result from defect dynamics.

The state of spiral defect chaos has received much attention as it shows unexpected chaotic behavior that is bistable at values of system parameters corresponding to the flow being stable and stationary [13–15]. A number of characterizations of the state have been made emphasizing local instabilities, wave vector frustration and mean flows that may be linked with defect nucleation [11,12,16–19]. Here, we report on two characterizations of the state that quantify the geometric structure of the flow in spiral defect chaos. First, we determine the distribution of the area of distinct convection roll structures. Second, we reduce the patterns exhibited by the system to a graph. This parametrizes the system through the number of nearest-neighbors of each distinct roll. These measures characterize the topology and packing of the striped patterns observed within the convective region and provide unique insights into the underlying dynamics.



Figure 1. A typical image of the convective state exhibiting spiral defect chaos (at $\epsilon = 2.82$) as visualized using shadowgraphy. The convective fluid is bounded horizontally in a circular domain with radius 3.8 cm and vertically extends to about 0.69 mm.

One of the most prominent features of the dynamics of convection rolls is their incessant merger and pinch-off. As a result of such dynamics, two distinct neighboring rolls become a single larger roll (during merger) or a single roll splits in two (during pinch-off) with each newly formed distinct roll being smaller than the original roll. If such dynamics occurs randomly along any position along the roll, on average it would result in the size of a roll doubling during merger or halving during pinch-off. A schematic of this process is shown in figure 2. Since each such event leads to the size of a roll changing by a factor of two, we study the distribution of roll sizes in base two. A similar argument may be made for the number of nearest-neighbors as illustrated in figure 2.

2. Experimental set-up

Our experiments use compressed carbon dioxide as the convective fluid. The gas is held in a convection cell bounded below by a 1 cm thick gold plated aluminium mirror and above by a 2 cm thick transparent sapphire crystal. The lateral boundaries comprise of stacks of filter papers 0.069 cm thick that also act as a spacer between the upper and lower boundaries. The filter paper has a 3.8 cm diameter circular hole in the center within which the convection is visualized. The aluminium mirror has a resistive thin film heater attached to it on the bottom and rests on high precision screws that may be turned to align the mirror. The mirror is levelled with respect to the sapphire window using laser interferometry. Chilled water at a controlled temperature is circulated over the top of the sapphire window to maintain its temperature. In addition, thermistors embedded in the side of the aluminium mirror as well as close to the sapphire plate are used to monitor the temperature gradient across the convective layer. The set-up is contained within an aluminium canister pressurized to 30 atm with CO₂ gas using an external pressurized cylinder. Computer control of the thin film heater is used to set the temperature difference,



Figure 2. A schematic of roll pinch-off and merger for a set of rolls participating in defect nucleation is shown. During this process, the two dark rolls merge, leading to the number of distinct dark rolls halving from 2 to 1. At the same time, the lighter colored rolls split, doubling their number from 1 to 2. Concurrent with this, the size of the distinct darker roll has approximately doubled while that of the lighter roll has halved. The number of nearest-neighbors in this ideal case of parallel alignment of rolls has also been increased from 1 light roll to 2 light rolls, and vice versa for the dark rolls. The physics of such dynamics therefore motivates studying distributions of roll sizes and nearest-neighbor distributions in base 2.

T , between the top and bottom boundary of the convective cell to within 10 mK of the desired value. Our experimental set-up is further detailed and characterized in [20].

At a critical temperature difference across the fluid, $T = T_c$, the onset of convection occurs resulting in the formation of roll-like structures. The visualization of the convective rolls is done using shadowgraphy [21,22]. This technique utilizes the variation in the refractive index between hot and cold regions of the gas to focus light differently. The images are captured using a CCD camera with high and low intensities representing hotter upflows and cooler downflows.

We set our experiment at different values of the reduced Rayleigh number, $\epsilon = [T - T_c]/T_c$. A sequence of 18000 images acquired at 11 Hz are used in our data analysis. We capture the dynamics of the system over many times the vertical thermal diffusion time (about 2 s in our system), which is the time scale at which defect nucleation occurs resulting in topological changes within the pattern. The distributions reported in this manuscript are stationary over the observation time. The response of the system falls qualitatively into three regimes [5,23]: $0 \leq \epsilon \leq 0.5$, where the convective rolls are stationary states of the system; $0.5 \leq \epsilon \leq 1.5$ results in the onset of time dependence and weak turbulence, and $1.5 \leq \epsilon$ shows prominent time-dependent chaotic behavior.

3. Image processing

A background image of the fluid flow prior to the onset of convection is subtracted from every image to compensate stationary optical inhomogeneities from irregularities in the optical path. These difference images are Fourier filtered to eliminate

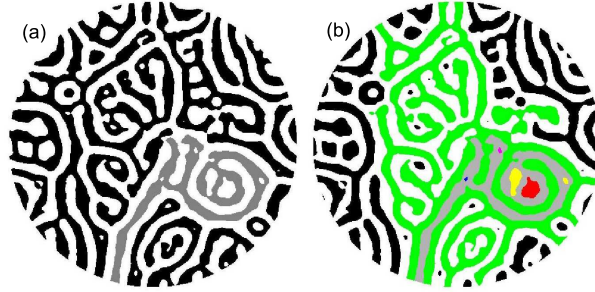


Figure 3. (a) A set of convection rolls representing the dark areas of figure 1 are indicated by dark regions of a binary image. As an example of a distinct component of this flow, one of the rolls that is singly connected is shaded in gray. (b) The complementary flow is shown, representing the bright areas in figure 1. In addition, the gray component is added for visual effect, while also indicating its nearest-neighbors in color.

the influence of high frequency noise associated with the CCD array as well as low frequency variations associated with nonuniform illumination. The intensity profile of the resultant image is representative of the structure of the convective rolls. The image is thresholded at the median value of intensity to yield a binary image. This choice of a threshold segregates the convective region into equal areas representing hot upflows and cold downflows to be consistent with the conservation of mass.

The segregation of the flow into two distinct components as depicted by the binary image (figure 3) provides the basis for our characterizations. A similar approach based on algebraic topology has been used to characterize patterns [24]. As illustrated in figure 3a, each distinct bright (dark) roll is completely surrounded by dark (bright) rolls, or the boundary of the convective cell.

4. Distribution of area/length of stripes

In the first characterization, we simply look at the area of distinct bright or dark rolls as a fraction of the total convective area. A normalized distribution of the number of distinct rolls at a given ϵ is plotted in figure 4. Since the convective rolls have a well-defined average width, the area of the rolls is well-approximated by a constant scalar multiple of the length of the roll. The convective rolls may be looked upon as primarily one-dimensional curves within the circular convective region. At the lower values of area, this distribution is cut-off when the length of a convective roll equals its width. The diameter of the cell bounds the maximum area of straight roll. However, curvature and mergers between rolls can result in rolls of length exceeding the cell diameter.

The kinks in figure 4a–c occur at an area corresponding to that of a roll with length equal to the diameter of the convective region. There is a sharp drop in the number of rolls that have a length greater than the diameter of the convection cell. This is because the rolls are without much curvature at lower values of ϵ . At higher values of ϵ , the roll curvature increases, leading to a smoother distribution of roll

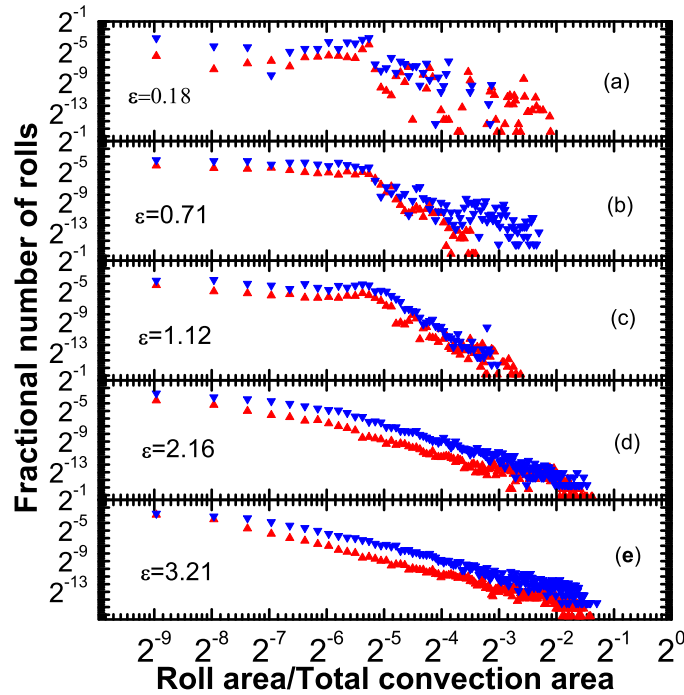


Figure 4. The distributions of the number of convective rolls at a given area fraction is plotted with increasing values of ϵ . At large values of ϵ , the data is well-fit by a straight line. In plot (e), a linear fit corresponds to a line of slope -1.81 ± 0.03 . Bright and dark regions are distinguished by upward and downward pointing triangles.

sizes. The distinction between the distributions for upflows and downflows is due to non-Boussinesq effects and has been thoroughly investigated in [20,25].

The kink in the distribution is retained over the observation time, but is less dominant with increasing ϵ . The number of defects that nucleate within the pattern increases with time. However, the spatial density of these nucleations increases with increasing ϵ . This indicates that the distribution of roll lengths overcomes the influence of the cell diameter with increasing density of defects rather than the number of defects that occurs in the pattern.

At higher values of ϵ , the distribution plotted in figure 4 is well-fit by a straight line. Convergence to this distribution indicates that the optimal packing of the rolls within the finite aspect-ratio cell is achieved with a power-law distribution in roll sizes within the range observed. The sizes of contiguous rolls change due to pinch-off and merger of rolls. On an average, these processes are expected to halve or double the number as well as areas of contiguous regions. Hence, we use base 2 as physically relevant to plot the distribution in figure 4. An interesting study would be to estimate if the current distributions continue to hold at larger aspect ratios.

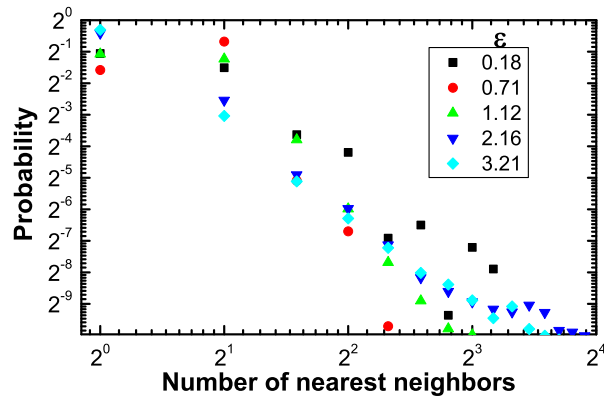


Figure 5. The variation of the number of nearest-neighbors is shown at different temperature gradients across the fluid. At high values of ϵ , the distribution is fit by a straight line. The slope when $\epsilon = 3.21$ is -2.61 ± 0.05 .

5. Nearest-neighbor distributions

A further topological characterization may be made by considering the binary image of the flow as a bipartite graph. To do this, we count the number of distinct bright rolls, each contiguous dark roll shares an interface with and vice versa. Each bright (dark) roll may be considered as a vertex connected to its nearest-neighbor along its boundary to a corresponding dark (bright) roll/vertex. Figure 3b illustrates this measurement by indicating the nearest-neighbors of a single convective roll in the flow (indicated in gray). In our binary image, bright (dark) regions are surrounded by dark (bright) regions with the only exceptions being at the boundaries. We count the number of nearest-neighbors of every dark (bright) region that is bright (dark). A set of numbers representing the average number of nearest neighbors for each distinct dark/bright region is thus generated at a constant value of ϵ . We normalize this set to unity to compute the probability of having a given average number of nearest-neighbors. This quantity is plotted against the number of nearest-neighbors for a convective roll as shown in figure 5. These probabilities converge to a distribution well-fit by a straight line at high ϵ .

The probability of having only one neighbor is finite for rolls that are at the boundary, or are completely encircled by a different roll. There is a general trend for the number of rolls with two nearest-neighbors to decrease with increasing ϵ as in figure 5. In the simple geometries of parallel stripes and target patterns, the number of nearest-neighbors is two. When more complex patterns emerge, they can often be broken down into spatially localized regions with simple geometries. For example, the statistical distributions of spirals (identified by eye) in the state was studied analogous to magnetic spin [26]. The present characterization develops a general technique to make global and rigorous characterizations of the system based on the nearest-neighbor distributions within the flow.

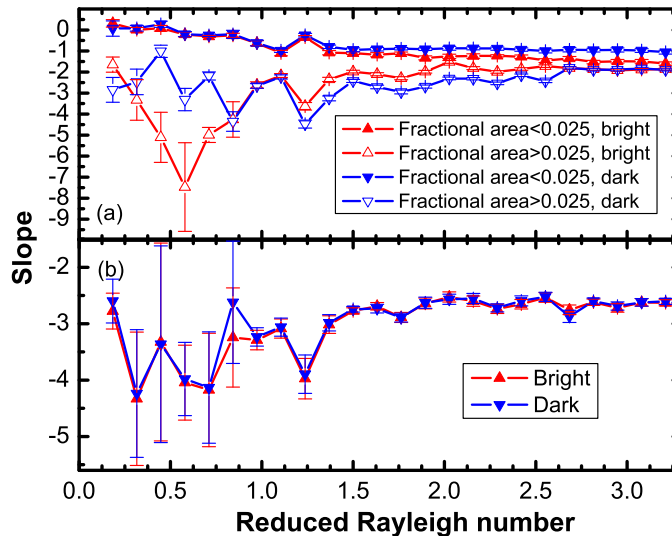


Figure 6. The variation of the slopes from least-squares fit to straight lines as parametrizing the distributions in figures 4a and 5b as a function of ϵ . A distribution is well-fit by a straight line when the error in the extracted slope is small.

6. Variation with Rayleigh number

At higher values of ϵ , the distributions of nearest-neighbors are also well-fit by a straight line in the log-log plot of figure 5. While the lengths of rolls show a sharp kink associated with the system size, there is no feature corresponding to this in the nearest-neighbor distributions. The distribution of the area of the system are metric-dependent, and correspondingly show an associated length scale of the system size. The nearest-neighbor distributions, however, are metric-independent and a topological measure of the intertwining of the rolls. The two measures are related as they determine the packing of upflows and downflows in the system.

The distributions quantifying the areas as well as the nearest-neighbor distributions of convective rolls converge with increasing ϵ as seen in figure 6. Here, the slopes of lines used to fit the distributions are indicated along with their error-bars. When the error bars are large, the distributions are not well-fit by a straight line. At larger values of ϵ , the small error bars indicate convergence to a straight line. However, this convergence is not monotonic. We believe this may be related to frustration arising between the shapes of the stripes (described by the wavelength, curvature, length of rolls etc) and the finite system size. A varying shape of the rolls with ϵ could lead to a frustrated packing for the rolls. A thorough investigation of this aspect is beyond the scope of the present investigation.

7. Conclusions

The present study develops characterizations of fluid flows that offer insightful comparisons with other complex systems characterized using similar measures. These include describing small world networks, structure of the internet and protein-protein interactions [27–29].

In spiral defect chaos, the extreme confinement of the fluid between the top and bottom plates primarily determines the wave number exhibited by the system. This results in a bounded distribution of power in Fourier space, corresponding to the wavelength of the convective rolls. We find that while the wave vectors are constrained, the length distribution of the rolls and topological measures characterizing the nearest-neighbor distributions converge to suggest power-law distributions that may occur in an infinite system. The distributions are stationary and do not change as the number of defects the system is subjected to increases at a given Rayleigh number. Therefore, we also conjecture that the final distributions are not the outcome of the number of defects the system is subjected to, but the density of defects that changes with Rayleigh number.

Acknowledgements

The author would like to thank M F Gameiro, K Mischaikow, N Przulj and J D Scheel for useful discussions. In addition, the author is grateful to M F Schatz in whose laboratory the experiments were carried out. This work was supported by the Institute for Complex Adaptive Matter.

References

- [1] Lord Rayleigh, *Philos. Mag.* **32**, 529 (1916)
- [2] F H Busse, *J. Fluid Mech.* **30**, 625 (1967)
- [3] Eberhard Bodenschatz, Werner Pesch and Guenter Ahlers, *Ann. Rev. Fluid Mech.* **32**, 708 (2000)
- [4] S Chandrasekhar, *Hydrodynamic and hydromagnetic stability*, International Series of Monographs on Physics (Dover Publications, Oxford, England, 1981)
- [5] V Croquette, *Contemp. Phys.* **30(2)**, 113 (1989)
- [6] Stephen W Morris, Eberhard Bodenschatz, David S Cannell and Guenter Ahlers, *Phys. Rev. Lett.* **71(13)**, 2026 (1993)
- [7] Hao Wen Xi, J D Gunton and Jorge Vinals, *Phys. Rev. Lett.* **71(13)**, 2030 (1993)
- [8] W Decker, W Pesch and A Weber, *Phys. Rev. Lett.* **73(5)**, 648 (1994)
- [9] K Krishan, Network structure of spiral defect chaos, arXiv:0705.1993, May 2007
- [10] K Krishan, A Handel, R O Grigoriev and M F Schatz, Modal extraction in spatially extended systems, arXiv:0704.1011, April 2007
- [11] Werner Pesch, David A Egolf, Ilarion V Melnikov and Robert E Ecke, *Nature (London)* **404**, 733 (2000)
- [12] David A Egolf, Ilarion V Melnikov and Eberhard Bodenschatz, *Phys. Rev. Lett.* **80(15)**, 3228 (1998)
- [13] Michel Assenheimer and Victor Steinberg, *Nature (London)* **367**, 345 (1994)

- [14] Kapil M S Bajaj, David S Cannell and Guenter Ahlers, *Phys. Rev.* **E55(5)**, R4869 (1997)
- [15] Reha V Cakmur, David A Egolf, Brendan B Plapp and Eberhard Bodenschatz, *Phys. Rev. Lett.* **79(10)**, 1853 (1997)
- [16] K-H Chiam, M R Paul, M C Cross and H S Greenside, *Phys. Rev.* **E67(5)**, 056206 (2003)
- [17] Hao Wen Xi, Xiao Jun Li and J D Gunton, *Phys. Rev. Lett.* **78(6)**, 1046 (1997)
- [18] M C Cross and Yuhai Tu, *Phys. Rev. Lett.* **75(5)**, 834 (1995)
- [19] Jun Liu and Guenter Ahlers, *Phys. Rev. Lett.* **77(15)**, 3126 (1996)
- [20] K Krishan, H Kurtuldu, M F Schatz and M Gameiro, *Phys. Fluids* **19**, 117105 (2007)
- [21] John R de Bruyn, Eberhard Bodenschatz, Stephen W Morris, Steven P Trainoff, Yuchou Hu, David S Cannell and Guenter Ahlers, *Rev. Sci. Instrum.* **67(6)**, 2043 (1996)
- [22] G S Settles, *Schlieren and shadowgraph techniques* (Springer, 2006)
- [23] Brendan Bryce Plapp, *Spiral pattern formation in Rayleigh–Bénard convection*, Ph.D. thesis (Cornell University, 1997)
- [24] Marcio Gameiro, Konstantin Mischaikow and William Kalies, *Phys. Rev.* **E70(3)**, 035203 (2004)
- [25] Santiago Madruga and Hermann Riecke, *Phys. Rev.* **E75(2)**, 026210 (2007)
- [26] Robert E Ecke, Yuchou Hu, Ronnie Mainieri and Guenter Ahlers, *Science* **269(2)**, 1704 (1995)
- [27] D J Watts and S Strogatz, *Nature (London)* **393**, 440 (1998)
- [28] Michalis Faloutsos, Petros Faloutsos and Christos Faloutsos, On power-law relationships of the internet topology, *SIGCOMM* (1999)
- [29] Ulrich Stelzl, *Cell* **122**, 957 (2003)